

1 **Growth patterns of caudal fin rays are informed by both external signals from the**
2 **regenerating organ and remembered identity autonomous to the local tissue**

3 Melody Autumn¹, Yinan Hu¹, Jenny Zeng¹, and Sarah K. McMenamin^{1‡}

4
5 ¹Biology Department, Boston College, Chestnut Hill, MA 02467

6 [‡]Author for correspondence: mcmenam@bc.edu, Higgins Hall 360, 140 Commonwealth
7 Avenue, Chestnut Hill, MA 02467

8
9 Author contributions: M.A., Y.H., and S.K.M. designed research; M.A., Y.H., and J.Z. performed
10 research; M.A., Y.H., and S.K.M. analyzed data; and M.A. and S.K.M. wrote the paper.

11
12
13 **ABSTRACT**

14 Regenerating tissues must remember or interpret their spatial position, using this information to
15 restore original size and patterning. The external skeleton of the zebrafish caudal fin is
16 composed of 18 rays; after any portion of the fin is amputated, position-dependent regenerative
17 growth restores each ray to its original length. We tested for transcriptional differences during
18 regeneration of proximal versus distal tissues and identified 489 genes that differed in
19 proximodistal expression. Thyroid hormone directs multiple aspects of ray patterning along the
20 proximodistal axis, and we identified 364 transcripts showing a proximodistal expression pattern
21 that was dependent on thyroid hormone context. To test what aspects of ray positional identity
22 are directed by extrinsic cues versus remembered identity autonomous to the tissue itself, we
23 transplanted distal portions of rays to proximal environments and evaluated regeneration within
24 the new location. While neighboring proximal tissue showed robust expression of *scpp7*, a
25 transcript with thyroid-regulated proximal enrichment, regenerating rays originating from
26 transplanted distal tissue showed reduced (distal-like) expression during outgrowth. These
27 distal-to-proximal transplants regenerated far beyond the length of the graft itself, indicating that
28 cues from the proximal environment promoted additional growth. Nonetheless, these transplants
29 initially regenerated at a much slower rate compared to controls, suggesting memory of distal
30 identity was retained by the transplanted tissue. This early growth retardation caused rays that
31 originated from transplants to become noticeably shorter than their native neighboring rays.
32 While several aspects of fin ray morphology (bifurcation, segment length) were found to be
33 determined by the environment, regeneration speed and ray length are remembered
34 autonomously by tissues, persisting across multiple rounds of amputation and regeneration.

35
36 **KEYWORDS**

37 Regeneration, Zebrafish, Transplant, Growth rate, Skeletal patterning, Thyroid hormone

38 INTRODUCTION

39

40 To restore the original morphology of an appendage, regeneration must faithfully rebuild lost
41 tissue. The morphology and size to which regenerating tissue grows must be determined by
42 positional information (Wolpert, 1969). Such cues could be informed by remembered positional
43 identity or could be interpreted from environmental cues from surrounding tissue (e.g. diffusible
44 or spatially distributed factors). However, these two potential inputs can be difficult to
45 disentangle.

46 Zebrafish fins are powerful models for studying regeneration and can provide new
47 insights into the nature of positional memory and the pathways that regulate regional growth
48 and patterning. The caudal fin is made up of symmetrical dorsal and ventral lobes, each
49 composed of nine segmented fin rays. Upon amputation, a blastema of de-differentiated cells
50 forms (Knopf et al., 2011; Tu & Johnson, 2011), and each ray regrows from the wound site to
51 rebuild its original morphology (reviewed in Harris et al., 2021; I. M. Sehring & Weidinger, 2020).

52 Regeneration rate is informed by the relative proximodistal location of the regenerating
53 tissue on the fin (Lee et al., 2005). Distal amputations are followed by slow regenerative growth,
54 while proximal amputations close to the body initiate rapid growth that progressively slows as
55 the regenerate approaches the original size (Akimenko et al., 1995; Banu et al., 2022; Lee et al.,
56 2005; Uemoto et al., 2020). Regardless of how much tissue is removed, regeneration restores
57 the organ to its original size within three weeks (Wehner et al., 2014).

58 Intact fin rays exhibit morphological differences along the proximodistal axis. At the
59 proximal base, ray segments are longest and widest, tapering and shortening progressively
60 towards the distal edge; rays also form bifurcations at specific locations along the axis (Harper
61 et al., 2023). Components of proximodistal patterning are regulated by thyroid hormone (TH),
62 which induces distal features (Harper et al., 2023). Proximal and distal tissues from intact adult
63 fins show unique transcriptomic profiles (Rabinowitz et al., 2017), and these expression patterns
64 are regulated by developmental TH (Harper et al., 2023). Here, we tested if transcriptomic
65 differences are apparent during the regeneration of proximal compared to distal regions of the
66 fin.

67 The relative length of individual rays appears to be remembered autonomously by
68 tissues (Uemoto et al., 2020). Fin rays differ in length from the central to the peripheral regions
69 of the fin, giving the organ an overall forked shape. Previous transplantation experiments
70 demonstrate that when short central rays are swapped with long peripheral rays, the tissue
71 regenerating in the new environment produces a ray of intermediate length (Shibata et al.,
72 2018). However, it remains unclear whether proximodistal location along an intact ray imprints
73 remembered positional information that could inform morphology during regeneration.

74 Transplants of blastema cells from different proximodistal locations were not able to
75 influence lengths of regenerates (Shibata et al., 2018). Further, hemi-rays—the apposed
76 contralateral bones that make up individual ray segments—can be transplanted to different
77 proximodistal locations; the resulting recombinant rays regenerate with morphologies expected
78 for the regenerating environment (Murciano et al., 2007). Nonetheless, given the notable
79 differences in gene expression and morphology along the intact proximodistal axis, we asked if
80 entire ray segments could remember proximodistal identity, and we tested the ability of this
81 memory to influence gene expression, regrowth rates, ultimate length and patterning of
82 regenerating rays.

83

84 RESULTS

85

86 **Regenerating fin tissue shows unique proximodistal transcription.** Many genes show
87 proximodistal differences in expression as the caudal fin regenerates (Akimenko et al., 1995;
88 Lee et al., 2005), and we aimed to capture trends across the transcriptome during the

89 regeneration of the organ. Amputating at a consistent proximal location, we evaluated
90 expression from three regions as they regenerated a proximal region collected after the
91 blastema had already formed (Wang et al., 2019; 4 days post amputation, dpa), a middle region
92 midway through regeneration as the ray bifurcations were forming (7 dpa), and a distal region
93 (15 dpa; see Supplementary Fig. 1C). We identified 489 transcripts that were differentially
94 expressed between proximal and distal regenerating tissue (Fig. 1A-B): 29 genes were
95 proximally enriched and 460 were distally enriched. GO term analysis of differentially expressed
96 transcripts along the proximodistal axis showed enrichment of genes involved in pigmentation,
97 likely reflecting differentiation of pigment cells (Supplementary Fig. 1G). Transcripts dependent
98 on thyroid hormone were enriched for gas transport GO terms, potentially reflecting shifts in
99 circulation and metabolism (Supplementary Fig. 1H). In our regenerates, ray bifurcations were
100 actively forming during the middle time point (7 dpa); however, this tissue revealed no
101 transcripts that were differentially expressed compared to proximal and distal tissues.

102

103 **Hypothyroid tissues lose proximodistal differential expression of many genes.**

104 Developmental hypothyroidism proximalizes both transcriptional expression and ray morphology
105 in intact fins (Harper et al., 2023), and we asked if fins regenerating in a hypothyroid context
106 also showed proximalized gene expression patterns. We reasoned that transcripts with a TH-
107 regulated expression differential would be strong candidates as mediators of proximodistal
108 patterning and distal identity. Analyzing the transcriptomes holistically, the major axes of
109 variation robustly captured proximodistal location (dimension 1) and TH condition (dimension 2),
110 but there was little apparent correlation between the two (Fig. 1A). Nonetheless, certain
111 transcripts showed a proximodistal differential in expression that was dependent on the
112 presence of TH. Indeed, of the 489 differentially expressed genes found in WT tissue, 364 lost
113 proximodistal specificity in hypothyroid tissue: ~86% (25/29) of proximally enriched and ~76%
114 (349/460) of distally enriched genes lost proximodistal differential expression in a hypothyroid
115 context.

116

117 ***scpp7* is proximally enriched during regeneration.** Of the transcripts showing TH-dependent
118 proximal enrichment, secretory calcium-binding phosphoprotein 7 (*scpp7*) could be robustly
119 visualized using RNAscope (Fig 1D-E, G-H). Along with other SCPP factors, SCPP7 is involved
120 in bone mineralization (Kawasaki, 2009), and is strongly upregulated during scale regeneration
121 (Bergen et al., 2022). Proximal tissues showed robust expression of *scpp7* in both WT and
122 hypothyroid backgrounds, but the gene was more strongly expressed in distal tissue from
123 hypothyroid regenerates compared to those of WT (Fig. 1C-H).

124 We asked if the variation in *scpp7* expression in the different regions could be attributed
125 to differences in the time since injury rather than proximodistal position of regeneration. To test
126 this possibility, we performed distal amputations on WT fins (see Supplementary Fig. 1D) and
127 assessed *scpp7* expression in 4 dpa distally-regenerating tissue. *scpp7* expression was similar
128 to that of 15 dpa distally-regenerating tissues (Supplementary Fig. 1E-F), suggesting that this
129 expression differential indeed characterizes distal regenerating tissue.

130

131 ***scpp7* expression in regenerating tissues reflects original proximodistal location rather than regenerative environment.**

132 We asked whether attenuated *scpp7* expression would be remembered by distal tissues if they regenerated in a proximal context. To test this, we
133 designed a distal-to-proximal ray transplantation procedure in which a ray was removed from
134 the fin, and a distal portion of the extirpated ray was transplanted into the proximal position.
135 After the distal transplant integrated into the proximal location, the entire fin was amputated
136 (through the transplant) to allow distal tissue to regenerate alongside proximal tissue (“dist-to-
137 prox”, Fig. 2A-C; see Methods and Supplementary Fig. 10 for additional details). A completely
138 extirpated ray with no transplant produced no regeneration (Supplementary Fig. 2). We
139

140 assessed *scpp7* expression in the regenerate originating from the dist-to-prox transplant and
141 found expression was significantly reduced compared to those of neighboring proximal rays at 4
142 dpa (Fig. 2D-E). This recapitulation of distal-like expression while regenerating in a proximal
143 context suggests that expression level of this transcript is informed by original tissue identity.

144
145 **Distal-to-proximal transplanted tissue restores shorter fin rays.** We predicted that if dist-to-
146 prox transplanted tissue possessed remembered positional identity, precocious distal features
147 should be apparent in the resulting regenerate. To adequately evaluate subtle differences in
148 regrowth, we needed a comparison that had undergone identical microsurgery without
149 introducing a major axis translocation. Thus, we performed control “prox-to-prox” transplants,
150 extirpating a ray, then grafting the entire tissue back into its position (Fig. 3A-D). Interestingly,
151 these prox-to-prox rays were not able to regenerate to the same length as the corresponding
152 rays on the ventral lobe (Supplementary Fig. 3K) and were ultimately slightly shorter than
153 undisturbed neighboring rays. During microsurgery, prox-to-prox rays inevitably lost 1-3
154 segments and about a mm in length (Supplementary Fig. 3I), so the change in ultimate length
155 may reflect a slight positional shift. Additionally (or alternatively), the manipulation of the
156 microsurgery itself may be sufficient to effect patterns of regeneration.

157 Compared to the microsurgery-controlled baseline of prox-to-prox rays, rays originating
158 from dist-to-prox transplants were consistently shorter, through eleven weeks after amputation
159 (Fig. 3I). Dist-to-prox regenerates were obviously shorter than both neighboring rays (Fig. 3G-H)
160 and the corresponding ray on the ventral lobe (Supplementary Fig. 3G-H). These differences in
161 ultimate length suggest that the dist-to-prox transplants autonomously retain memory of their
162 original proximodistal identity.

163
164 **Growth rates during regeneration reflect both intrinsic identity and environmental**
165 **context.** Since the dist-to-prox regenerates were significantly shorter compared to prox-to-prox
166 regenerates, we asked whether these regenerates grew at a relatively slower pace. During the
167 first week of regeneration (weeks 0-1), prox-to-prox transplants regenerated rapidly, adding 2.6
168 mm (0.37 mm per day); in contrast, dist-to-prox regenerates grew much more slowly, adding
169 only 2.0 mm during this first week (0.27 mm per day; Fig. 3J-K). By the second week (weeks 1-
170 2), the two types of transplants were growing at comparable speeds, adding 1.9 mm length
171 (0.27 mm per day). Through the remainder of the eleven-week period, dist-to-prox and prox-to-
172 prox rays maintained similar regrowth speeds (Fig. 3J-K). Growth rates plateaued after week
173 nine, as the regenerates reached isometric growth (Fig. 3J-K). Prox-to-prox rays’ regrowth
174 speed was reduced in comparison to corresponding ventral rays during the first week of
175 regeneration but by the second week they kept pace (Supplementary Fig. 3J-K).

176
177 **Fin ray patterning is environmentally coordinated.** Bifurcations are a discrete indicator of
178 proximodistal morphology (Harper et al., 2023). We asked whether the origin of tissue (distal
179 versus proximal) would influence the location of the bifurcation in a regenerate, and we
180 quantified the bifurcation position in dist-to-prox and prox-to-prox rays. Bifurcations formed in
181 the location expected for the environment regardless of transplant type (Fig. 4C), suggesting
182 bifurcation position is the result of globally coordinated cues (Dagenais et al., 2021; Murciano et
183 al., 2002, 2007) rather than being locally regulated by tissues based on remembered identity.

184 **In evaluating appropriate controls for our dist-to-prox transplants, we discovered that**
185 while ray length is similar between dorsal and ventral lobes, the proximodistal patterning differs
186 between the dorsal and ventral lobes of uninjured fins (Supplementary Fig. 4). Further,
187 regenerated ray segments were somewhat longer and wider than segments of the intact fin,
188 with bifurcations farther from the body (Supplementary Fig. 5E-F; Supplementary Fig. 6I-J; also
189 see Azevedo et al., 2012). Therefore, we the prox-to-prox transplants were used as the best
190 comparisons for dist-to-prox proximodistal patterning. While dist-to-prox rays regrew marginally

191 thinner segments, segment length was comparable to that of prox-to-prox ray segments (Fig.
192 4D-E).

193 The total length of a regenerating fin can be increased by treating with a calcineurin
194 inhibitor, but these treatments do not alter positional memory and rays return to their WT
195 baseline upon regeneration (Daane et al., 2018). We asked if regenerating from a
196 pharmacologically-lengthened segment would alter the patterning of a regenerating ray;
197 however, once calcineurin inhibition was removed, segment length and location of bifurcation
198 were indistinguishable from control regenerates (Supplementary Fig. 8).

199
200 **Rays originating from distal transplants remember their length through multiple rounds**
201 **of regeneration.** To test whether the intermediate length of dist-to-prox rays would be
202 remembered, we performed multiple rounds of regeneration, amputating distal to the previous
203 amputation plane (Fig. 5A-D). Even after three rounds of regeneration, rays originating from
204 dist-to-prox transplants were always significantly shorter than corresponding ventral rays (Fig.
205 5E-G).

206 207 **DISCUSSION**

208
209 Intact fins show transcriptomic differences across the proximodistal axis (Harper et al., 2023;
210 Rabinowitz et al., 2017), and here we identified a suite of genes that shift as the fin regenerates
211 different proximodistal regions. Previous transcriptomic analyses of regenerating fins have
212 focused on the early shifts in expression as the tissue initiates regenerative regrowth (Li et al.,
213 2021; Nauroy et al., 2019); we found that there are substantial shifts in expression patterns
214 even after regeneration is underway, corresponding with different stages of outgrowth proceed
215 (see Akimenko et al., 1995; Lee et al., 2005). Indeed, we found ten times as many distally- as
216 compared to proximally-enriched transcripts; this may reflect the increased number of
217 differentiated cells in the more mature regenerate (Nauroy et al., 2019).

218 The presence of TH throughout development distalizes gene expression patterns as fins
219 develop (Harper et al., 2023); however, during regeneration, hypothyroidism did not proximalize
220 pattern of gene expression. It is possible that temporal shifts in the regenerating transcriptome
221 overwhelmed any TH-dependent proximodistal pathways in our analysis, since the three stages
222 analyzed vary in both time since injury and proximodistal regions of regeneration. Nevertheless,
223 we identified many genes expressed in a proximodistal differential that was dependent on TH,
224 and these are strong candidates for mediators of distal patterning. Notably, we did not identify
225 any genes or pathways that were differentially expressed in the middle of the fin where
226 bifurcations formed. This suggests that there are not unique pathways underlying bifurcation,
227 and that expression patterns become progressively distalized as the proximodistal axis grows.

228 We showed that proximally-transplanted distal portions of zebrafish fin ray tissue
229 produced regenerates that were informed by retained memory of their original distal identity.
230 Regenerates originating from dist-to-prox transplants retained a distal pattern of gene
231 expression for a proximally-enriched transcript, initiated regeneration at a markedly slower pace,
232 and regrew to a shorter length than expected for their location. Dist-to-prox transplanted rays
233 regenerated much longer than the original size of the transplanted tissue, indicating that the
234 proximal environment can induce considerable growth in a regenerate. Notably however, dist-to-
235 prox regenerates grew to an ultimately much shorter length than was appropriate for their
236 regenerating environment, and this altered length was remembered through multiple rounds of
237 regeneration. In contrast to the regenerate length, however, we found no evidence that
238 proximodistal patterning was remembered by dist-to-prox transplanted tissue, as these
239 produced regenerates with segment patterning and bifurcation placement appropriate for their
240 environmental context.

241 Speed of regeneration is specific to proximodistal location: proximal tissue regrows
242 quickly while distal tissue regrows at a slower rate (Banu et al., 2022; Lee et al., 2005; Uemoto
243 et al., 2020). Dist-to-prox transplanted rays regenerated at a slower pace during the first week of
244 regrowth, suggesting a retained memory of distal identity. Thinner, smaller dist-to-prox rays
245 provide fewer cells for the initial proliferation of the blastema; this smaller pool of cells may
246 depress the initial speed of regeneration and ultimately shorten the total regenerated ray length
247 through multiple rounds of regeneration (as in Wang et al., 2019).

248 Although fin rays are known to retain memory of their original length (Shibata et al.,
249 2018), the existence of remembered identity along the proximodistal axis of the fin rays has not
250 previously been demonstrated. Previous proximodistal transplants of blastema cells or hemi-
251 rays did not demonstrate any retained memory of these tissues, however these transplants
252 grafted a much smaller portion of distal tissue (Murciano et al., 2007; Shibata et al., 2018, see
253 experimental setup diagram in Supplementary Fig. 9). There may be a threshold cell number
254 required to specify proximodistal identity not met in these previous experiments. Our dist-to-prox
255 transplantation relocates large numbers of numerous cell types, presumably including
256 osteoblasts, fibroblasts, ectoderm, blood vessels, nerve tissue and other cell types—intra-ray
257 fibroblasts are the likely mediators of positional information (Perathoner et al., 2014). Our
258 transplant translocated sufficient types and/or numbers of cells into a proximal location to
259 permanently alter positional memory in the regenerate.

260

261 SUMMARY

262

263 In all, regenerating caudal fins show progressive changes in expression along the proximodistal
264 axis, and many of these progressive changes are dependent on TH. We have shown that
265 proximodistal gene expression patterns can be remembered autonomously by fin tissues, with
266 dist-to-prox transplants producing regenerates with attenuated, distally-appropriate levels of
267 *scpp7* expression. Initial rates of regenerative growth are further informed by remembered
268 tissue identity: dist-to-prox rays begin regeneration at a slow (distally appropriate) rate. This
269 early setback maintains the ray originating from the transplant at a shorter length than
270 neighboring rays, and this decrease in length is remembered even through multiple rounds of
271 regeneration.

272

273 MATERIALS AND METHODS

274

275 **Fish rearing conditions.** Zebrafish were reared at 28°C with a 14:10 light:dark cycle.
276 Hypothyroid fish and their WT controls were *Tg(tg:nVenus-2a-nfnB)* (McMenamin et al., 2014).
277 All other fish were WT (Tübingen line). WT fish were fed marine rotifers, *Artemia*, Gemma Micro
278 (Skretting, Stavanger, NOR) and Adult Zebrafish Diet (Zeigler, Gardners PA, USA) 2-3 times
279 per day. Hypothyroid fish and their WT controls were fed a diet of Spirulina flakes (Pentair,
280 London, UK) and live *Artemia*.

281

282 **Thyroid follicle ablations.** To generate hypothyroid individuals, we performed transgenic
283 thyroid ablations (as in McMenamin et al., 2014). Briefly, to ablate the thyroid follicles of
284 *Tg(tg:nVenus-2a-nfnB)*, 4-5dpf larvae were incubated overnight in 10 mM metronidazole
285 (Thermo Scientific Chemicals) dissolved in 1% dimethyl sulfoxide (DMSO, Sigma) in larval
286 water, and controls with just 1% DMSO in larval water.

287

288 **RNA Sequencing.** Regenerating caudal fin tissue was collected from sibling adults (>18
289 standard length; SL) reared under wildtype or hypothyroid conditions during regeneration of
290 three different regions. To minimize enrichment of genes involved in blastema formation (Li et
291 al., 2021; Nauroy et al., 2019), we chose 4 dpa regenerates to represent proximal outgrowth.

292 Tissue was collected at 4 dpa (proximal tissue), 7 dpa (middle tissue) or 15 dpa (distal
293 tissue). Fish were anesthetized with tricaine (MS-222, Pentair; ~0.02% w/v in system water), the
294 distal-most portion of the regenerating fin (~3 segments closest to the leading edge) was
295 collected and immediately flash frozen in a dry ice / ethanol bath. Three or four biological
296 replicates, each containing tissue from six individual fins, were collected at each time point and
297 TH condition. Total RNA was extracted immediately with Zymo Quick-RNA Microprep kit R1050
298 (Zymo Research, Irvine CA, USA). Quality check, library preparation, and sequencing were
299 performed by Genewiz (Cambridge, MA). Sample libraries were made with Illumina Truseq RNA
300 Library Prep kit and sequenced on an Illumina HiSeq platform with 150bp paired-end sequence
301 reads. Raw sequence reads were aligned to Zebrafish GRCz11 using STAR version 2.7.3 and
302 gene counts were called with Ensembl GRCz11 gene annotation. Differential gene expression
303 analyses were performed with Bioconductor package limma (Michaud et al., 2008). All
304 transcriptomes were analyzed by a multidimensional scaling plot to detect overall differences in
305 the transcriptomes. Subsequently, comparisons were made between proximal and distal
306 regenerating regions in both WT and hypothyroid backgrounds; these were subsequently
307 compared to identify the subset of differentially expressed genes that lost differential expression
308 in a hypothyroid context. Genes were considered significantly expressed if they showed a \log_2
309 fold difference higher than 2 and a false discovery rate lower than 0.01.

310
311 **Microsurgeries.** Transplantation was most reliable using larger adults, so all individuals used
312 for microsurgies were 25-40mm SL. For ray extirpation, the interray tissue on both sides of
313 dorsal ray four (DR4) was cut (using Surgical Grade Blades #11) to separate the ray from its
314 neighbors. The entire ray was then plucked from the peduncle, by securing the zebrafish body
315 with General-Purpose Broad-Tipped Forceps (Fisher Scientific) while using Dumont #5 Forceps
316 (Fine Science Tools, 1125240) to grasp the base of the ray. For dist-to-prox transplants, DR4
317 was extirpated from the fin, ~2 mm of the distal tip was clipped off, and this portion was grafted
318 back into the now-empty DR4 site (see Supplementary Fig. 10 for further detail). For prox-to-
319 prox transplants, DR4 was extirpated and then re-inserted in its native position. Directly after
320 transplantation, fish were maintained in a lightly anesthetized state for 30-60 minutes using
321 ~0.01% tricaine and 3PPM clove bud oil (Sigma-Aldrich). One day post-transplant, we assessed
322 fins for graft success: dist-to-prox transplants grafted ~80% of the time while prox-to-prox
323 transplants only grafted in ~60% of microsurgies. After allowing 24 hours for recovery and for
324 the graft to fuse with neighboring tissues, fish were again anesthetized with tricaine, and the
325 entire fin (including the transplanted graft) was amputated along a single plane with a razor
326 blade.

327
328 **RNAscope whole mount *in situ* hybridization.** Regenerating fins were collected at 4 dpa
329 (proximal tissue or dist-to-prox tissue) or 15 dpa (distal tissue) and fixed for 30 minutes in 4%
330 PFA at room temperature. Fins were stained as described in (I. Sehring et al., 2022) with the
331 modification that all 0.2x SSCT washes were only performed twice. We used the RNAscope
332 Multiplex Fluorescent Reagent Kit v2 (ACD Bio-technie, 323100) to screen seven candidate
333 probes (ACD Bio-technie: *scpp7* 1265951-C1, *rhbg* 1315181-C2, *kcnma1a* 1315191-C3, *nfil3-6*
334 1265961-C2, *noxo1a* 1265971-C3, *defbl1* 1265981-C4, *olfml2ba* 1315201-C4) in proximal and
335 distal regenerating tissue. Only the *scpp7* probe was able to reliably label transcripts in our
336 whole mount tissues. Selecting candidates with known function, gene targets were manually
337 curated from the 45 transcripts that showed proximal or distal enrichment was dependent upon
338 TH.

339
340 **Imaging.** Zebrafish were anesthetized with tricaine and imaged on an Olympus SZX16
341 stereoscope with an Olympus DP74 camera or an Olympus IX83 inverted microscope with a
342 Hamamatsu ORCA Flash 4.0 camera. Identical microscope settings (including exposure and

343 magnification) were used for all samples within each fluorescent *in situ* experiment. Images
344 were transformed in FIJI with the Fire LUT for visualization. For fluorescent quantifications, we
345 used FIJI to capture mean fluorescent intensity at the distal end of dorsal ray three, dorsal ray
346 four transplant, and dorsal ray five (DR3, DR4, and DR5).

347
348 **Analyses.** All analyses were done in R 4.2.2. DR4 was used for all transplant procedures, with
349 non-transplanted ventral ray four (VR4) serving as an internal comparison. Any damaged rays
350 were excluded from analysis. Fin ray morphology was quantified with the StereoMorph R
351 package (Olsen & Westneat, 2015) as described in (Harper et al., 2023). We used paired or
352 unpaired Welch two-sample t tests or a paired repeated samples ANOVA followed by pairwise *t*
353 tests to account for the two rays from a single fin or multiple time points assessed. Significance
354 was marked as: $p < 0.05$, *; $p < 0.01$, **; $p < 0.001$, ***.

355
356 **Pharmacological treatments.** FK506 (Selleck Chemicals) was suspended in DMSO, then
357 diluted to 200 nM FK506 and 0.02% DMSO. Controls were treated with 0.02% DMSO. ~70%
358 water changes were performed every other day throughout the treatment before washout. Fish
359 recovered for seven days, then were amputated a second time with no drug treatment.

360 361 **AKNOLWEDGEMENTS**

362 Thank you to all McMenamin Lab members past and present for fish care assistance. For data
363 analysis support, we thank Melissa McTernan. For R assistance and dino nuggets, we thank
364 Brian Autumn. For critical input and discussion, we thank Eric Folker, Matthew Harris, Vicki
365 Losick and the anonymous reviewers of the manuscript.
366 Funding provided by NSF CAREER 1845513 and NIH R35GM146467 (S.K.M.).

367 368 **REFERENCES**

- 369 Akimenko, M. A., Johnson, S. L., Westerfield, M., & Ekker, M. (1995). Differential induction of four
370 *msx* homeobox genes during fin development and regeneration in zebrafish. *Development*,
371 *121*(2), 347–357.
- 372 Azevedo, A. S., Sousa, S., Jacinto, A., & Saúde, L. (2012). An amputation resets positional
373 information to a proximal identity in the regenerating zebrafish caudal fin. *BMC Developmental*
374 *Biology*, *12*, 24. <https://doi.org/10.1186/1471-213X-12-24>
- 375 Banu, S., Gaur, N., Nair, S., Ravikrishnan, T., Khan, S., Mani, S., Bharathi, S., Mandal, K., Kuram, N.
376 A., Vuppaladadium, S., Ravi, R., Murthy, C. L. N., Quoseena, M., Babu, N. S., & Idris, M. M.
377 (2022). Understanding the complexity of epimorphic regeneration in zebrafish caudal fin
378 tissue: A transcriptomic and proteomic approach. *Genomics*, *114*(2), 110300.
379 <https://doi.org/10.1016/J.YGENO.2022.110300>
- 380 Bergen, D. J. M., Tong, Q., Shukla, A., Newham, E., Zethof, J., Lundberg, M., Ryan, R., Youlten, S. E.,
381 Frysz, M., Croucher, P. I., Flik, G., Richardson, R. J., Kemp, J. P., Hammond, C. L., & Metz, J. R.
382 (2022). Regenerating zebrafish scales express a subset of evolutionary conserved genes
383 involved in human skeletal disease. *BMC Biology* *20*:1, *20*(1), 1–25.
384 <https://doi.org/10.1186/S12915-021-01209-8>
- 385 Crawford, K., & Stocum, D. L. (1988). Retinoic acid proximalizes level-specific properties
386 responsible for intercalary regeneration in axolotl limbs. *Development*, *104*(4), 703–712.
387 <https://doi.org/10.1242/DEV.104.4.703>

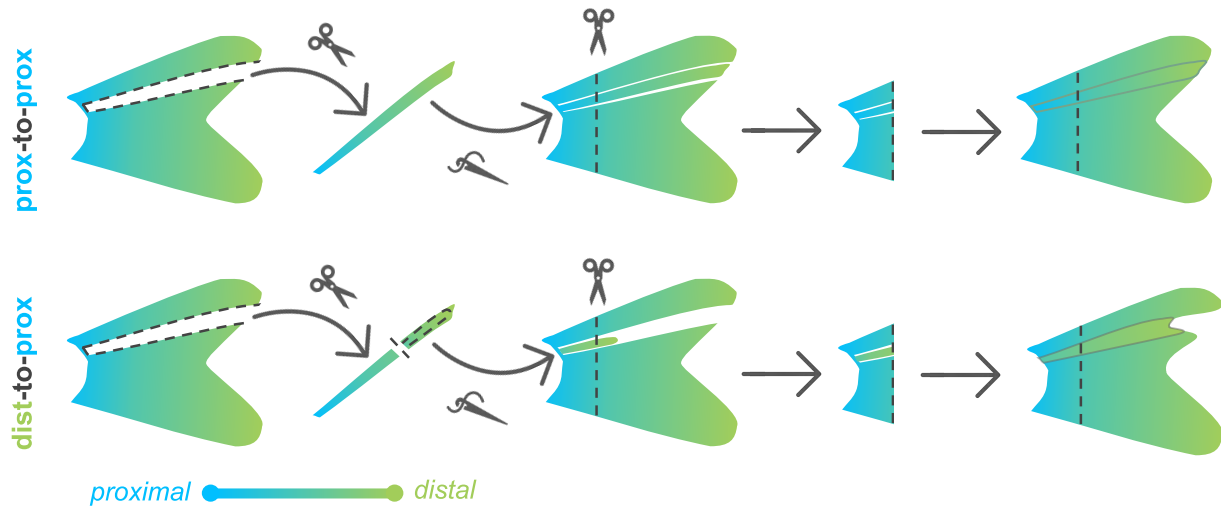
- 388 Daane, J. M., Blum, N., Lanni, J., Boldt, H., Iovine, M. K., Higdon, C. W., Johnson, S. L., Lovejoy, N. R.,
389 & Harris, M. P. (2021). Modulation of bioelectric cues in the evolution of flying fishes. *Current*
390 *Biology*, 31(22), 5052-5061.e8. <https://doi.org/10.1016/J.CUB.2021.08.054>
- 391 Daane, J. M., Lanni, J., Rothenberg, I., Seebohm, G., Higdon, C. W., Johnson, S. L., & Harris, M. P.
392 (2018). Bioelectric-calcineurin signaling module regulates allometric growth and size of the
393 zebrafish fin. *Scientific Reports* 2018 8:1, 8(1), 1–9. [https://doi.org/10.1038/s41598-018-](https://doi.org/10.1038/s41598-018-28450-6)
394 28450-6
- 395 Dagenais, P., Blanchoud, S., Pury, D., Pfefferli, C., Aegerter-Wilmsen, T., Aegerter, C. M., &
396 Jazwinska, A. (2021). Hydrodynamic stress and phenotypic plasticity of the zebrafish
397 regenerating fin. *Journal of Experimental Biology*, 224(15).
398 [https://doi.org/10.1242/JEB.242309/269186/AM/HYDRODYNAMIC-STRESS-AND-](https://doi.org/10.1242/JEB.242309/269186/AM/HYDRODYNAMIC-STRESS-AND-PHENOTYPIC-PLASTICITY-OF)
399 PHENOTYPIC-PLASTICITY-OF
- 400 Harper, M., Hu, Y., Donahue, J., Acosta, B., Braes, F. D., Nguyen, S., Zeng, J., Barbaro, J., Lee, H., Bui,
401 H., & Mcmenamin, S. K. (2023). Thyroid hormone regulates proximodistal patterning in fin rays.
402 *Proceedings of the National Academy of Sciences*, 120(21), e2219770120.
403 <https://doi.org/10.1073/PNAS.2219770120>
- 404 Harris, M. P., Daane, J. M., & Lanni, J. (2021). Through veiled mirrors: Fish fins giving insight into size
405 regulation. *Wiley Interdisciplinary Reviews: Developmental Biology*, 10(4).
406 <https://doi.org/10.1002/WDEV.381>
- 407 Kawasaki, K. (2009). The SPP gene repertoire in bony vertebrates and graded differences in
408 mineralized tissues. *Development Genes and Evolution*, 219(3), 147.
409 <https://doi.org/10.1007/S00427-009-0276-X>
- 410 Knopf, F., Hammond, C., Chekuru, A., Kurth, T., Hans, S., Weber, C. W., Mahatma, G., Fisher, S.,
411 Brand, M., Schulte-Merker, S., & Weidinger, G. (2011). Bone regenerates via dedifferentiation of
412 osteoblasts in the zebrafish fin. *Developmental Cell*, 20(5), 713–724.
413 <https://doi.org/10.1016/j.devcel.2011.04.014>
- 414 Kujawski, S., Lin, W., Kitte, F., Börmel, M., Fuchs, S., Arulmozhivarman, G., Vogt, S., Theil, D., Zhang,
415 Y., & Antos, C. L. (2014). Calcineurin Regulates Coordinated Outgrowth of Zebrafish
416 Regenerating Fins. *Developmental Cell*, 28(5), 573–587.
417 <https://doi.org/10.1016/J.DEVCEL.2014.01.019>
- 418 Lee, Y., Grill, S., Sanchez, A., Murphy-Ryan, M., & Poss, K. D. (2005). Fgf signaling instructs position-
419 dependent growth rate during zebrafish fin regeneration. *Development*, 132(23), 5173–5183.
420 <https://doi.org/10.1242/DEV.02101>
- 421 Li, J., Sultan, Y., Sun, Y., Zhang, S., Liu, Y., & Li, X. (2021). Expression analysis of Hsp90α and
422 cytokines in zebrafish caudal fin regeneration. *Developmental & Comparative Immunology*,
423 116, 103922. <https://doi.org/10.1016/J.DCI.2020.103922>
- 424 Maden, M. (1982). Vitamin A and pattern formation in the regenerating limb. *Nature*, 295.

- 425 McMenamin, S. K., Bain, E. J., McCann, A. E., Patterson, L. B., Eom, D. S., Waller, Z. P., Hamill, J. C.,
426 Kuhlman, J. A., Eisen, J. S., & Parichy, D. M. (2014). Thyroid hormone-dependent adult pigment
427 cell lineage and pattern in zebrafish. *Science*, *345*(6202), 1358–1361.
428 <https://doi.org/10.1126/science.1256251>
- 429 Michaud, J., Simpson, K. M., Escher, R., Buchet-Poyau, K., Beissbarth, T., Carmichael, C., Ritchie,
430 M. E., Schütz, F., Cannon, P., Liu, M., Shen, X., Ito, Y., Raskind, W. H., Horwitz, M. S., Osato, M.,
431 Turner, D. R., Speed, T. P., Kavallaris, M., Smyth, G. K., & Scott, H. S. (2008). *Integrative analysis*
432 *of RUNX1 downstream pathways and target genes*. <https://doi.org/10.1186/1471-2164-9-363>
- 433 Murciano, C., Fernández, T. D., Durán, I., Maseda, D., Ruiz-Sánchez, J., Becerra, J., Akimenko, M. A.,
434 & Marí-Beffa, M. (2002). Ray–Interray Interactions during Fin Regeneration of *Danio rerio*.
435 *Developmental Biology*, *252*(2), 214–224. <https://doi.org/10.1006/DBIO.2002.0848>
- 436 Murciano, C., Pérez-Claros, J., Smith, A., Avaron, F., Fernández, T. D., Durán, I., Ruiz-Sánchez, J.,
437 García, F., Becerra, J., Akimenko, M. A., & Marí-Beffa, M. (2007). Position dependence of
438 hemiray morphogenesis during tail fin regeneration in *Danio rerio*. *Developmental Biology*,
439 *312*(1), 272–283. <https://doi.org/10.1016/j.ydbio.2007.09.026>
- 440 Nauroy, P., Guiraud, A., Chlasta, J., Malbouyres, M., Gillet, B., Hughes, S., Lambert, E., & Ruggiero,
441 F. (2019). Gene profile of zebrafish fin regeneration offers clues to kinetics, organization and
442 biomechanics of basement membrane. *Matrix Biology*, *75–76*, 82–101.
443 <https://doi.org/10.1016/J.MATBIO.2018.07.005>
- 444 Olsen, A. M., & Westneat, M. W. (2015). StereoMorph: an R package for the collection of 3D
445 landmarks and curves using a stereo camera set-up. *Methods in Ecology and Evolution*, *6*(3),
446 351–356. <https://doi.org/10.1111/2041-210X.12326>
- 447 Perathoner, S., Daane, J. M., Henrion, U., Seebohm, G., & Higdon, C. W. (2014). Bioelectric Signaling
448 Regulates Size in Zebrafish Fins. *PLoS Genet*, *10*(1), 1004080.
449 <https://doi.org/10.1371/journal.pgen.1004080>
- 450 Pescitelli, M. J., & Stocum, D. L. (1980). The origin of skeletal structures during intercalary
451 regeneration of larval *Ambystoma* limbs. *Developmental Biology*, *79*(2), 255–275.
452 [https://doi.org/10.1016/0012-1606\(80\)90115-3](https://doi.org/10.1016/0012-1606(80)90115-3)
- 453 Rabinowitz, J. S., Robitaille, A. M., Wang, Y., Ray, C. A., Thummel, R., Gu, H., Djukovic, D., Raftery,
454 D., Berndt, J. D., & Moon, R. T. (2017). Transcriptomic, proteomic, and metabolomic landscape
455 of positional memory in the caudal fin of zebrafish. *Proceedings of the National Academy of*
456 *Sciences of the United States of America*, *114*(5), E717–E726.
457 <https://doi.org/10.1073/pnas.1620755114>
- 458 Sehring, I. M., & Weidinger, G. (2020). Recent advancements in understanding fin regeneration in
459 zebrafish. *WIREs Developmental Biology*, *9*(1). <https://doi.org/10.1002/wdev.367>
- 460 Sehring, I., Mohammadi, H. F., Haffner-Luntzer, M., Ignatius, A., Huber-Lang, M., & Weidinger, G.
461 (2022). Zebrafish fin regeneration involve generic and regeneration-specific osteoblast injury
462 responses. *ELife*, *11*. <https://doi.org/10.7554/ELIFE.77614>

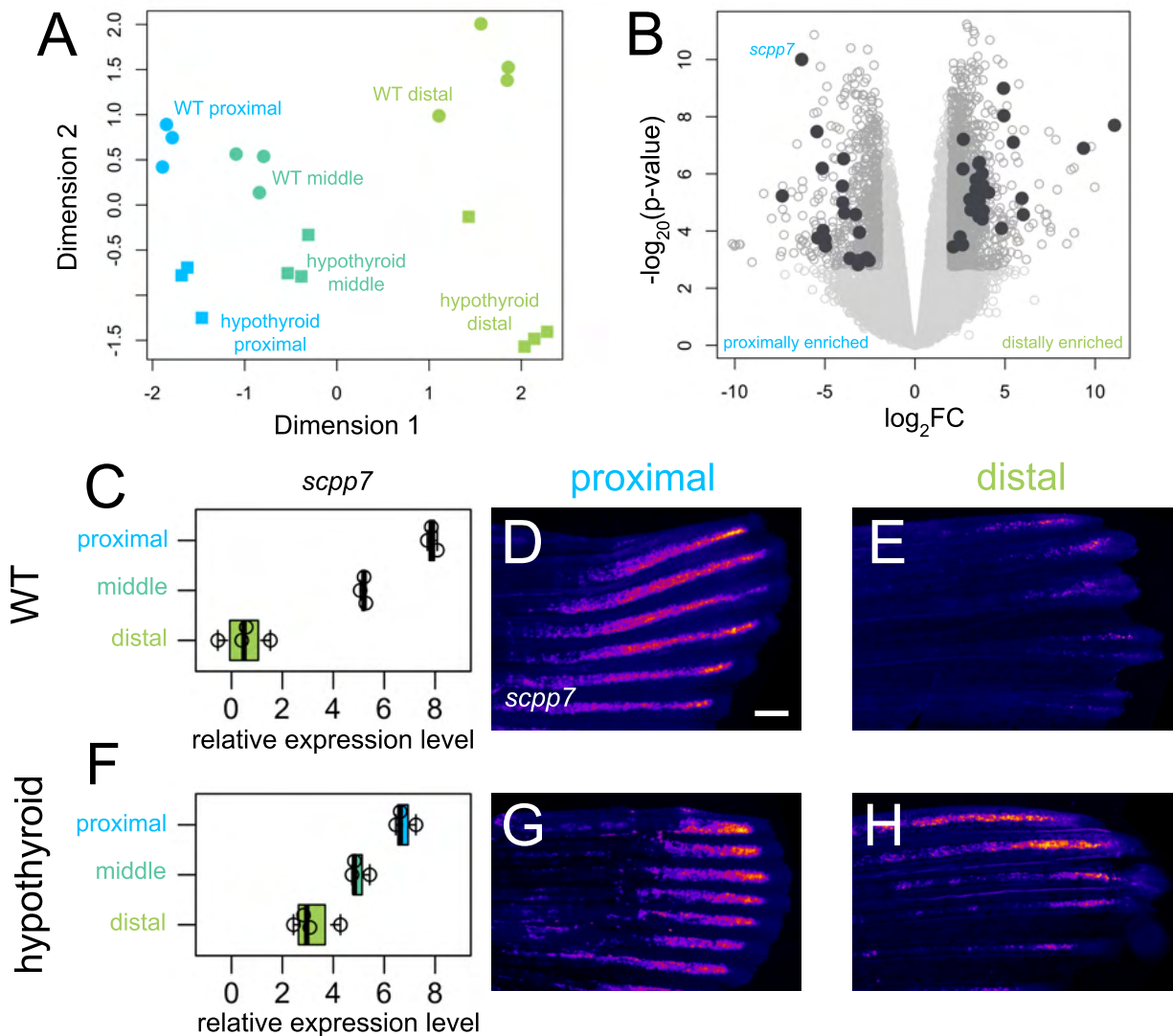
- 463 Shibata, E., Liu, Z., Kawasaki, T., Sakai, N., & Kawakami, A. (2018). Robust and local positional
464 information within a fin ray directs fin length during zebrafish regeneration. *Development*
465 *Growth and Differentiation*, 60(6), 354–364. <https://doi.org/10.1111/dgd.12558>
- 466 Stewart, S., Le Bleu, H. K., Yette, G. A., Henner, A. L., Robbins, A. E., Braunstein, J. A., & Stankunas,
467 K. (2021). longfin causes cis-ectopic expression of the *kcnh2a* ether-a-go-go K⁺ channel to
468 autonomously prolong fin outgrowth. *Development (Cambridge)*, 148(11).
469 <https://doi.org/10.1242/DEV.199384/260597/AM/LONGFIN-CAUSES-CIS-ECTOPIC->
470 [EXPRESSION-OF-THE](https://doi.org/10.1242/DEV.199384/260597/AM/LONGFIN-CAUSES-CIS-ECTOPIC-)
- 471 Stocum, D. L. (1984). The urodele limb regeneration blastema: Determination and organization of
472 the morphogenetic field. *Differentiation*, 27(1–3), 13–28. <https://doi.org/10.1111/J.1432->
473 [0436.1984.TB01403.X](https://doi.org/10.1111/J.1432-)
- 474 Tornini, V. A., Puliafito, A., Slota, L. A., Thompson, J. D., Nachtrab, G., Kaushik, A. L., Kapsimali, M.,
475 Primo, L., Di Talia, S., & Poss, K. D. (2016). Live Monitoring of Blastemal Cell Contributions
476 during Appendage Regeneration. *Current Biology*, 26(22), 2981–2991.
477 <https://doi.org/10.1016/j.cub.2016.08.072>
- 478 Tu, S., & Johnson, S. L. (2011). Fate restriction in the growing and regenerating zebrafish fin.
479 *Developmental Cell*, 20(5), 725–732. <https://doi.org/10.1016/j.devcel.2011.04.013>
- 480 Uemoto, T., Abe, G., & Tamura, K. (2020). Regrowth of zebrafish caudal fin regeneration is
481 determined by the amputated length. *Scientific Reports*, 10(1), 649.
482 <https://doi.org/10.1038/s41598-020-57533-6>
- 483 Wang, Y. T., Tseng, T. L., Kuo, Y. C., Yu, J. K., Su, Y. H., Poss, K. D., & Chen, C. H. (2019). Genetic
484 Reprogramming of Positional Memory in a Regenerating Appendage. *Current Biology*, 29(24),
485 4193–4207.e4. <https://doi.org/10.1016/j.cub.2019.10.038>
- 486 Wehner, D., Cizelsky, W., Vasudevaro, M. D., Özhan, G., Haase, C., Kagermeier-Schenk, B., Röder,
487 A., Dorsky, R. I., Moro, E., Argenton, F., Kühl, M., & Weidinger, G. (2014). Wnt/ β -catenin
488 signaling defines organizing centers that orchestrate growth and differentiation of the
489 regenerating zebrafish caudal fin. *Cell Reports*, 6(3), 467–481.
490 <https://doi.org/10.1016/j.celrep.2013.12.036>
- 491 Wolpert, L. (1969). Positional information and the spatial pattern of cellular differentiation. *Journal*
492 *of Theoretical Biology*, 25(1), 1–47. [https://doi.org/10.1016/S0022-5193\(69\)80016-0](https://doi.org/10.1016/S0022-5193(69)80016-0)
- 493 Yi, C., Spitters, T. W. G. M., Al-Far, E. A. D. A., Wang, S., Xiong, T., Cai, S., Yan, X., Guan, K., Wagner,
494 M., El-Armouche, A., & Antos, C. L. (2021). A calcineurin-mediated scaling mechanism that
495 controls a K⁺-leak channel to regulate morphogen and growth factor transcription. *ELife*, 10.
496 <https://doi.org/10.7554/ELIFE.60691>
- 497 Yin, V. P., Thomson, J. M., Thummel, R., Hyde, D. R., Hammond, S. M., & Poss, K. D. (2008). Fgf-
498 dependent depletion of microRNA-133 promotes appendage regeneration in zebrafish. *Genes*
499 *& Development*, 22(6), 728. <https://doi.org/10.1101/GAD.1641808>

501 **GRAPHICAL ABSTRACT**

502



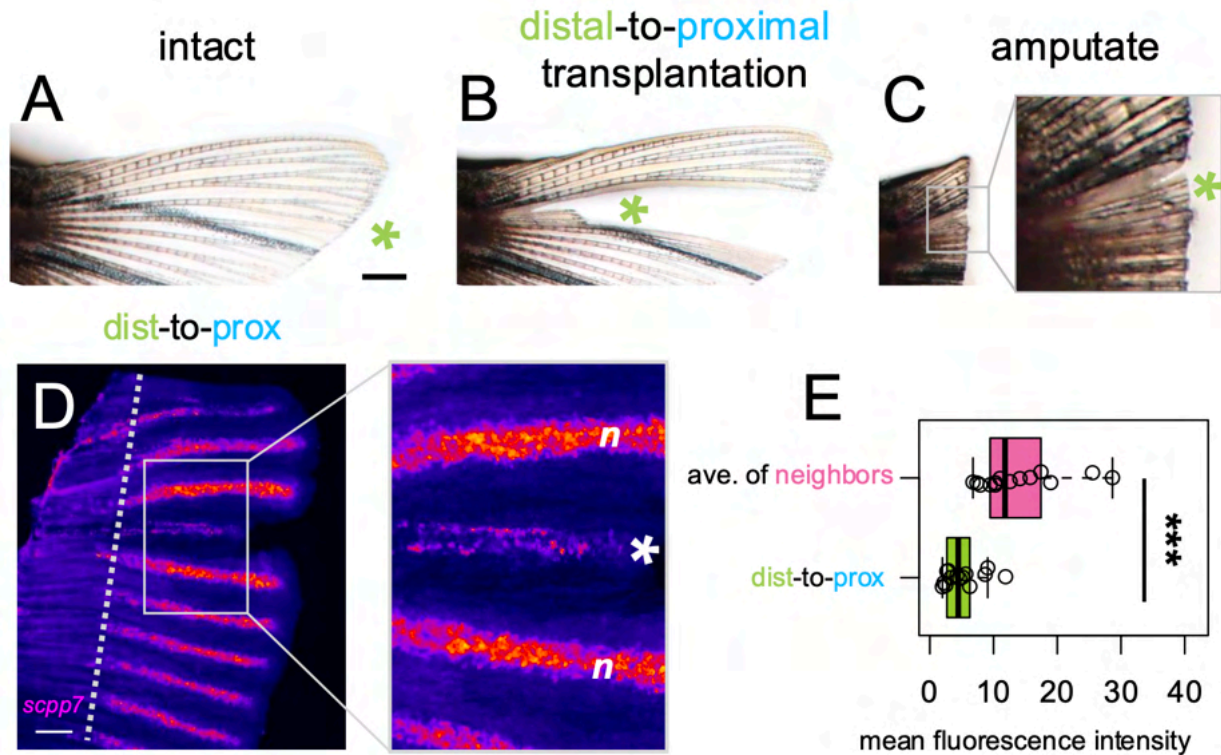
503



504

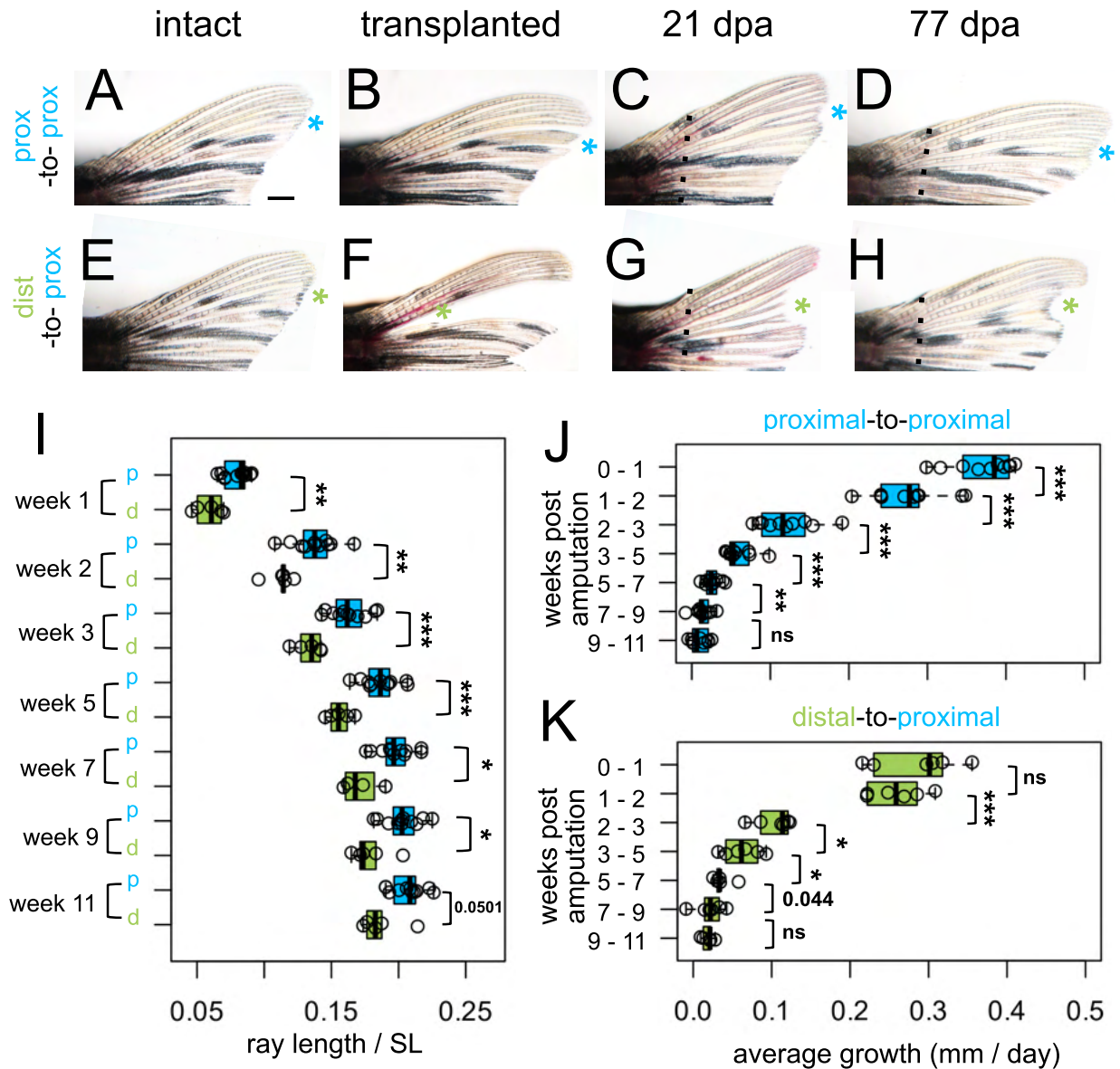
505 **Figure 1. Thyroid hormone distalizes gene expression patterns during regeneration.** (A)
506 Multidimensional scaling plot comparing gene expression profiles in different regions (proximal,
507 4 dpa; middle, 7 dpa; distal, 15 dpa) of regenerating tissue from WT and hypothyroid fish; each
508 data point represents one biological replicate. (B) Volcano plot showing differential gene
509 expression between regenerating proximal and distal regions in WT. Filled grey circles indicate
510 thyroid hormone-dependent genes. (D, F) *scpp7* relative expression in (C) WT and (F)
511 hypothyroid tissue samples. Note increased proximal expression in hypothyroid distal tissues.
512 Whole mount fluorescent *in situ* hybridization using custom *scpp7* RNAscope probe on (D-E)
513 WT and (G-H) hypothyroid tissue regenerating (D, G) proximal or (E, H) distal fin tissues. Warm
514 colors indicate highest regions of expression. Scale bar, 200 μm

515



516

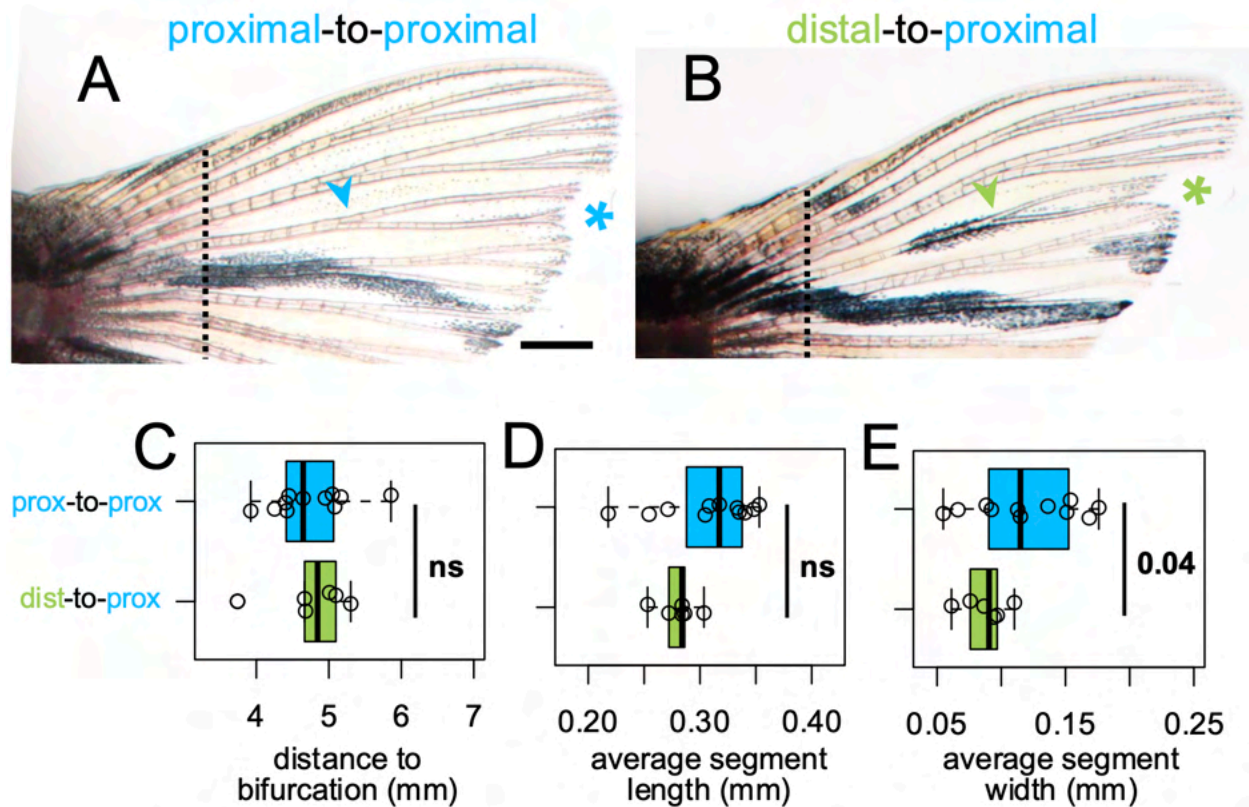
517 **Figure 2. *scpp7* expression in regenerating tissues reflects original position rather than**
518 **current environment.** (A-C) Example of a fin lobe subjected to the distal-to-proximal
519 transplantation procedure. (D) Whole mount fluorescent *in situ* hybridization with *scpp7*
520 RNA scope probe on dist-to-prox regenerating fins at 4 dpa. Warm colors indicate highest
521 regions of expression. (E) Boxplot showing mean fluorescence intensity of dist-to-prox
522 transplant tissue (asterisk) and the average intensity of its peripheral-most and center-most
523 neighbors (n). Significance determined by a Welch two-sample paired t test. Scale bars, (A) 1
524 mm; (D) 200 μ m.



525

526 **Figure 3. Regrowth rate reflects both intrinsic identity and the regenerative environment.**

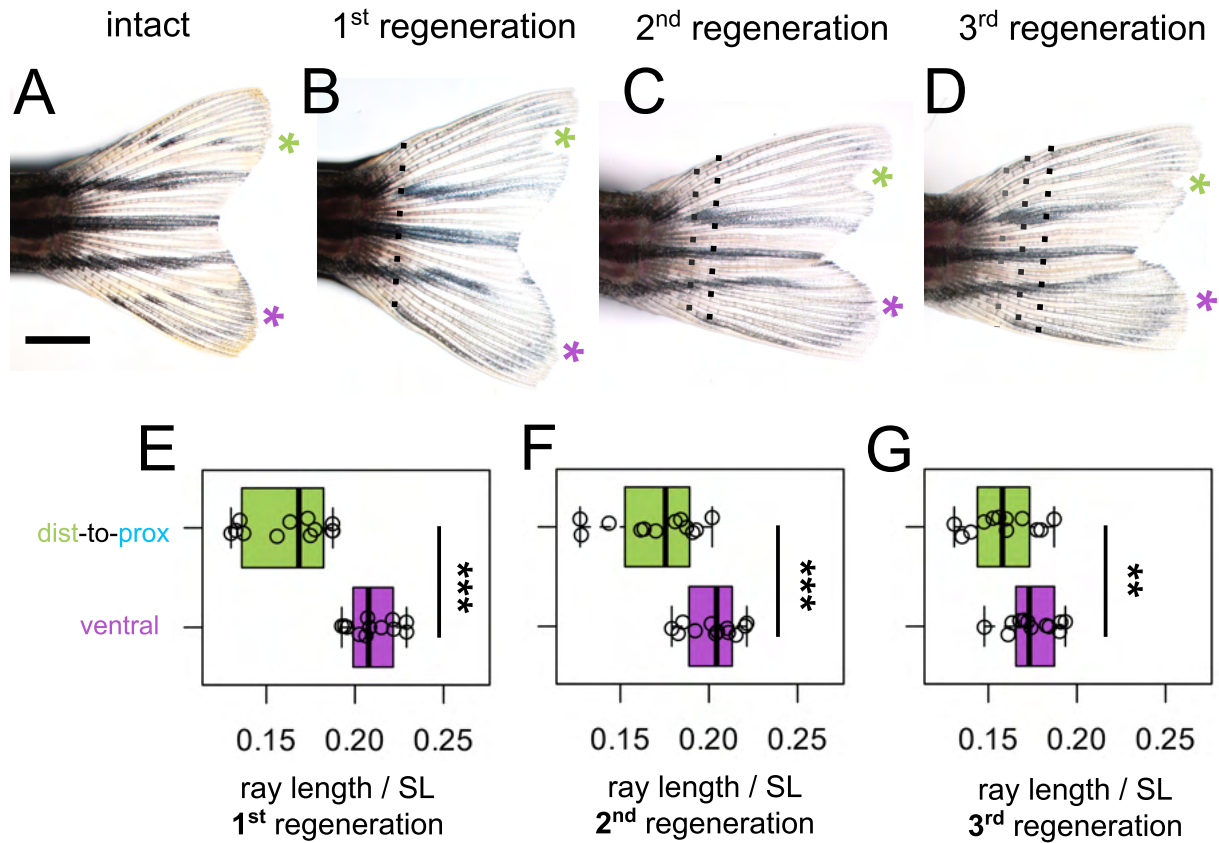
527 Dorsal fin lobes of (A-D) proximal-to-proximal (blue asterisk) or (E-H) distal-to-proximal (green
 528 asterisk) transplantation: (A, E) intact pre-transplantation, (B-F) one day post-transplantation,
 529 (C-G) regenerating at 21 dpa, (D, H) regenerating at 77 dpa. Amputation plane, dashed line. (I)
 530 Prox-to-prox versus dist-to-prox ray length (measured from amputation plane) normalized by
 531 standard length (SL) for each week. Average amount of growth per day during different growth
 532 periods for (J) prox-to-prox or (K) dist-to-prox rays. Significance determined by (J-K) paired or (I)
 533 unpaired Welch two-sample t tests. Scale bar, 1 mm.



534

535 **Figure 4. Fin ray patterning matches environment.** Dorsal fin lobe at 35dpa after either (A)
536 proximal-to-proximal (blue asterisk) or (B) distal-to-proximal (green asterisk) transplantation.
537 Amputation plane shown with dashed line. Arrowheads indicate primary bifurcations. Boxplots
538 showing the (C) proximodistal position of the bifurcation, (D) average segment length, and (E)
539 average segment width in regenerate. Significance determined by a Welch two-sample t test.
540 Scale bar, 1 mm.

541

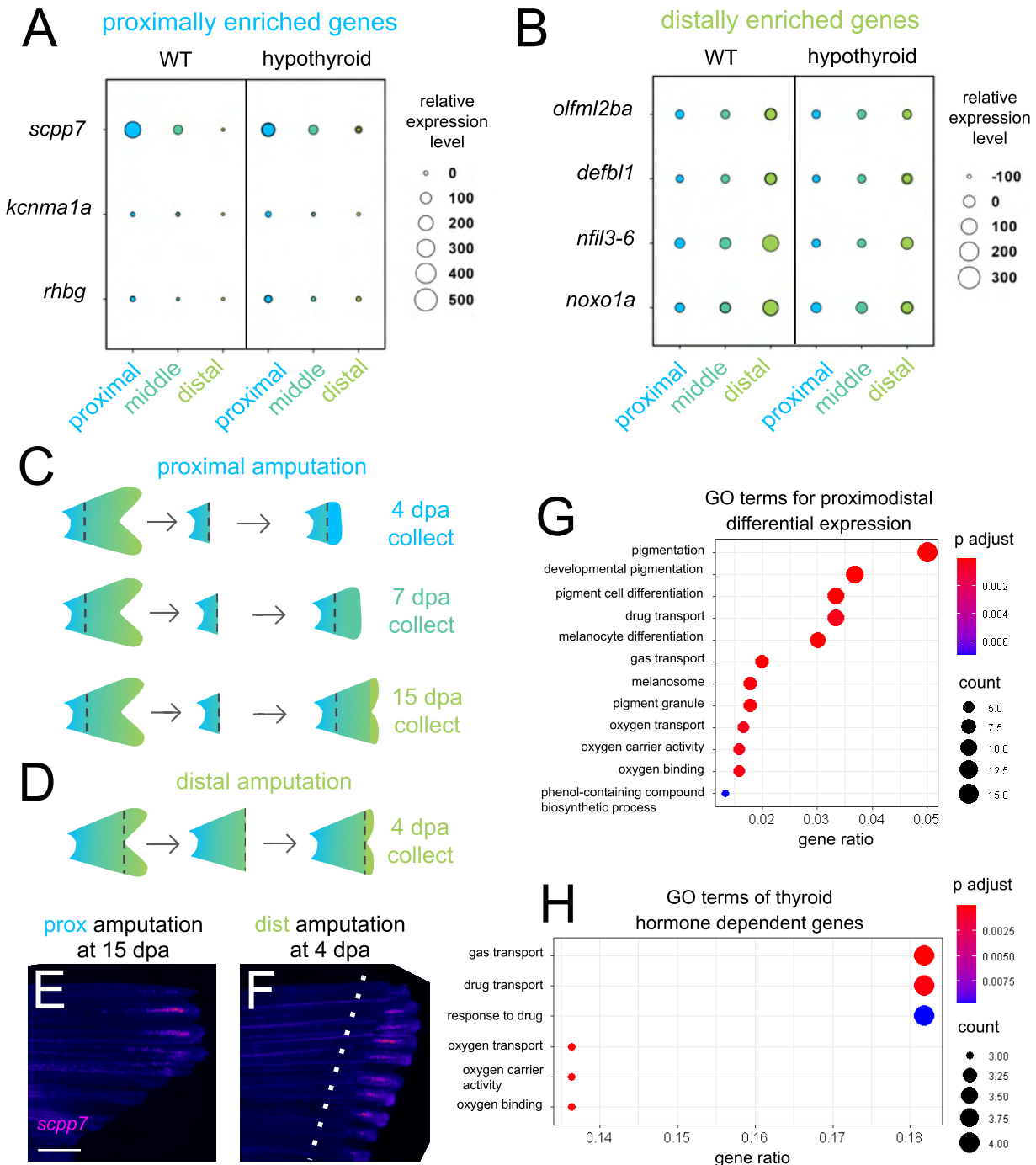


542

543 **Figure 5. Shorter ray length is remembered through multiple regeneration cycles.** (A)
544 Intact fin. (B-D) Regenerating fin after distal-to-proximal transplantation: (B) 28 days post first
545 amputation, (C) 28 days post second amputation, (C) 28 days post third amputation. Green
546 asterisk, dist-to-prox; purple asterisk, ventral ray. Black dashed line, most recent amputation.
547 Grey dashed lines, previous amputation planes. Boxplots showing the total length standardized
548 by SL after (E) first, (F) second, and (G) third regeneration. Ray length was measured from the
549 most recent amputation plane. Significance determined by paired Welch two-sample t test.
550 Scale bar, 2 mm.

551 **SUPPLEMENTARY FIGURES**

552

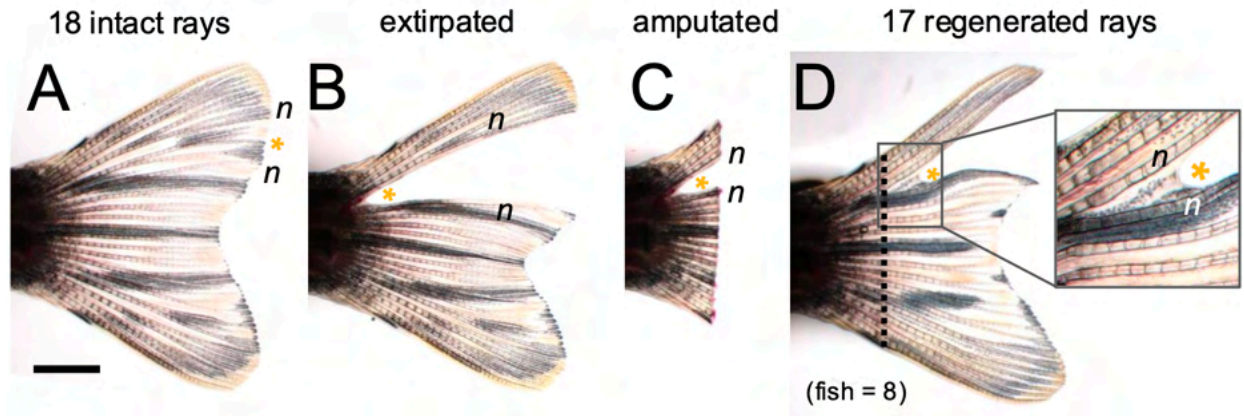


553

554 **Supplementary Figure 1. Differentially expressed gene candidates for fluorescent *in situ***
 555 **hybridization.** Thyroid hormone-dependent gene candidates that are either (A) proximally
 556 enriched or (B) distally enriched in WT tissues. Custom RNAscope probes were made and
 557 tested for all genes, but only the *scpp7* probe showed specific staining. (C-D) Schematic

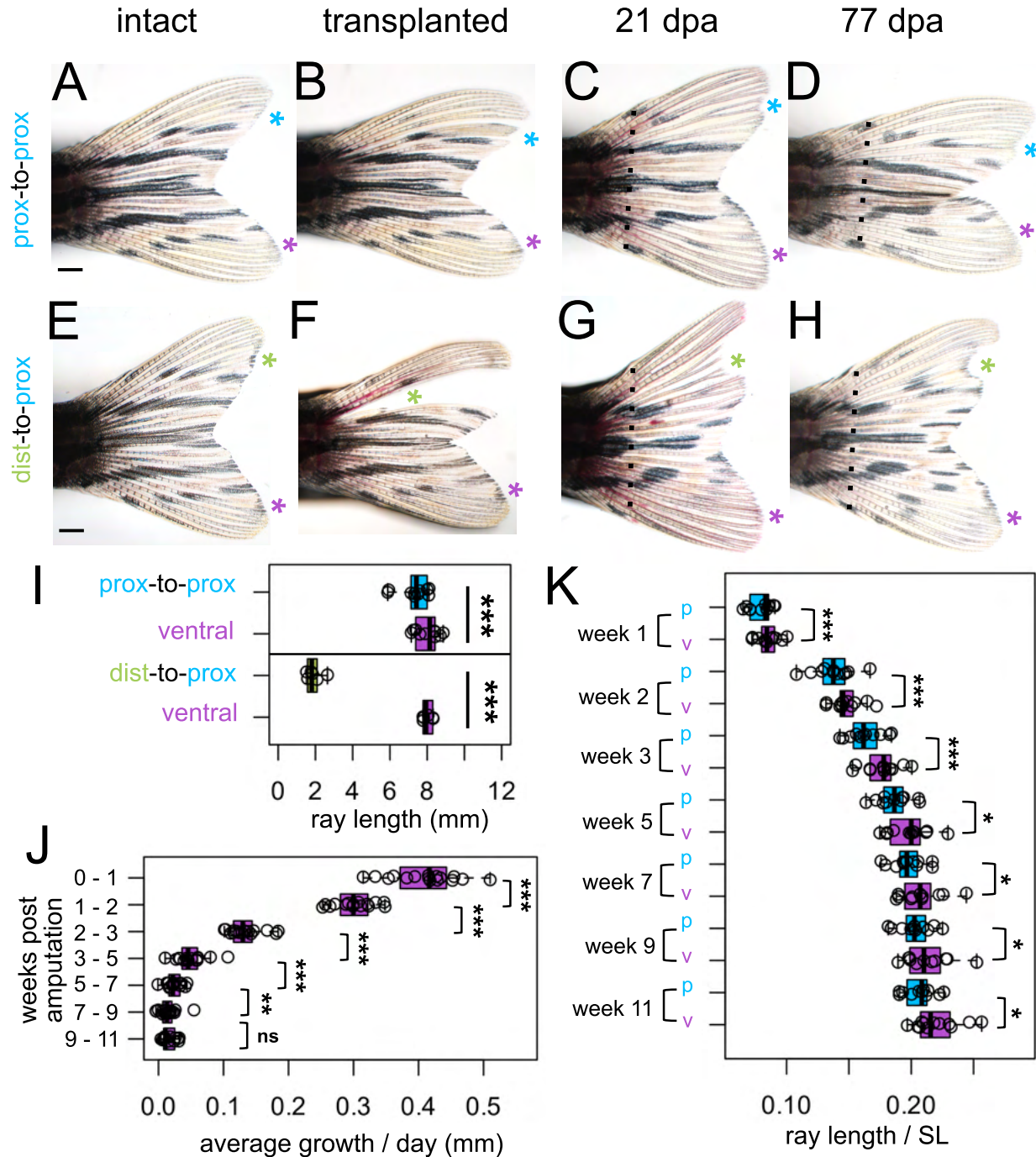
558 showing sample collection with (C) proximal or (D) distal amputation. (E) Proximally amputated
559 at 15dpa or (F) distally amputated 4dpa tissue stained for *scpp7*. Amputation plane, dashed line.
560 Warm colors indicate highest regions of expression. (G) GO enrichment of the 489 genes
561 proximodistal differentially expressed in WT. (H) GO enrichment of the 45 genes that were
562 thyroid hormone dependent and proximodistal differentially expressed in WT. Scale bar, 400 μ m.

563



564

565 **Supplementary Figure 2. Regeneration does not originate from an extirpated ray.** (A)
566 Intact fin with 18 rays, dorsal ray 4 (D4) marked with yellow asterisk. (B) Fin one day post D4
567 extirpation. (C) Freshly amputated fin, one day post D4 extirpation. (D) Fin regenerates with 17
568 rays (one-less ray than original, intact fin). n indicates neighboring dorsal rays 3 and 5.
569 Amputation plane, dashed line. Scale bar, 2 mm.



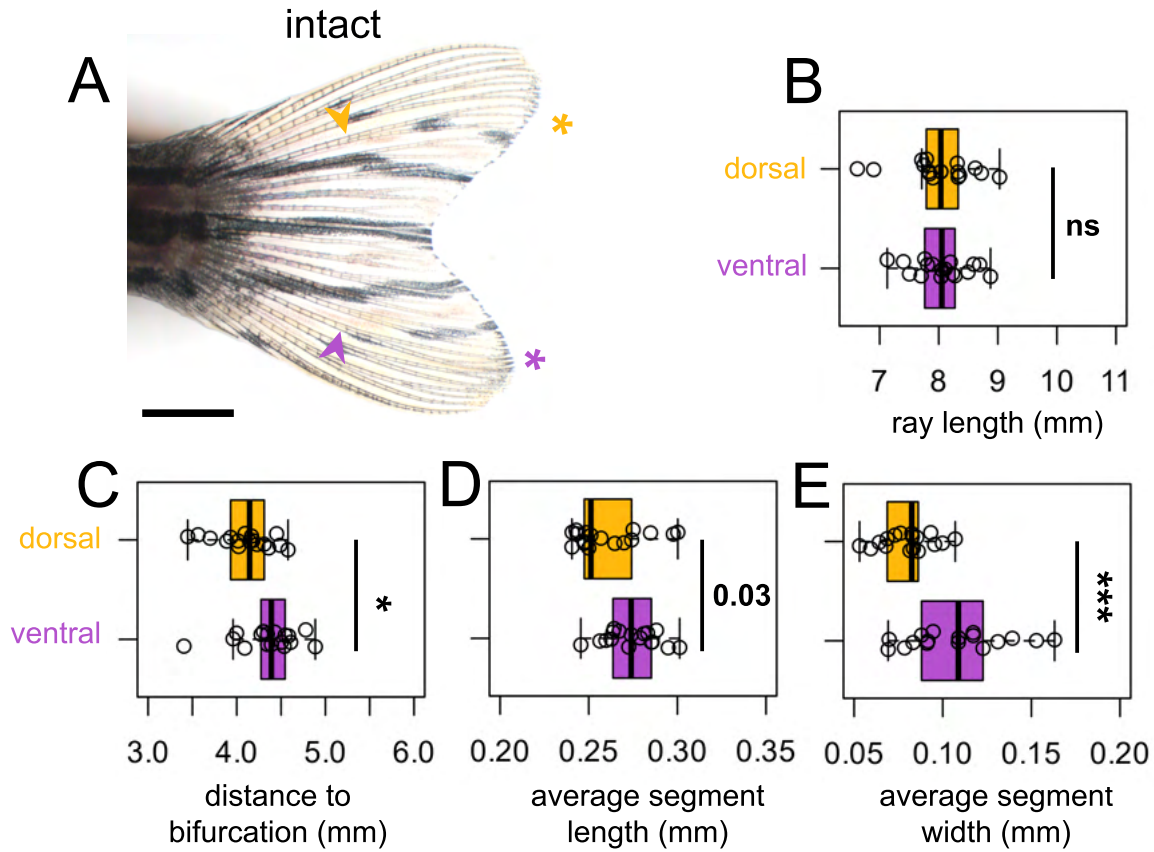
570

571 **Supplementary Figure 3. Non-transplanted rays regenerated faster than transplanted**
 572 **rays.** Fins of (A-D) proximal-to-proximal (blue asterisk) or (E-H) distal-to-proximal (green
 573 asterisk) transplantation: (A, E) intact pre-transplantation, (B-F) one day post-transplantation,
 574 (C-G) regenerating at 21 dpa, (D, H) regenerating at 77 dpa. Ventral rays indicated with purple
 575 asterisks. Amputation plane, dashed line. (I) Length of the rays after transplantation, as
 576 measured from the peduncle. (J) Average amount of growth per day during a one/two week
 577 periods for all the ventral ray comparisons. (K) Prox-to-prox rays versus ventral ray

578 comparisons, ray length (measured from amputation plane) divided by SL at each week.

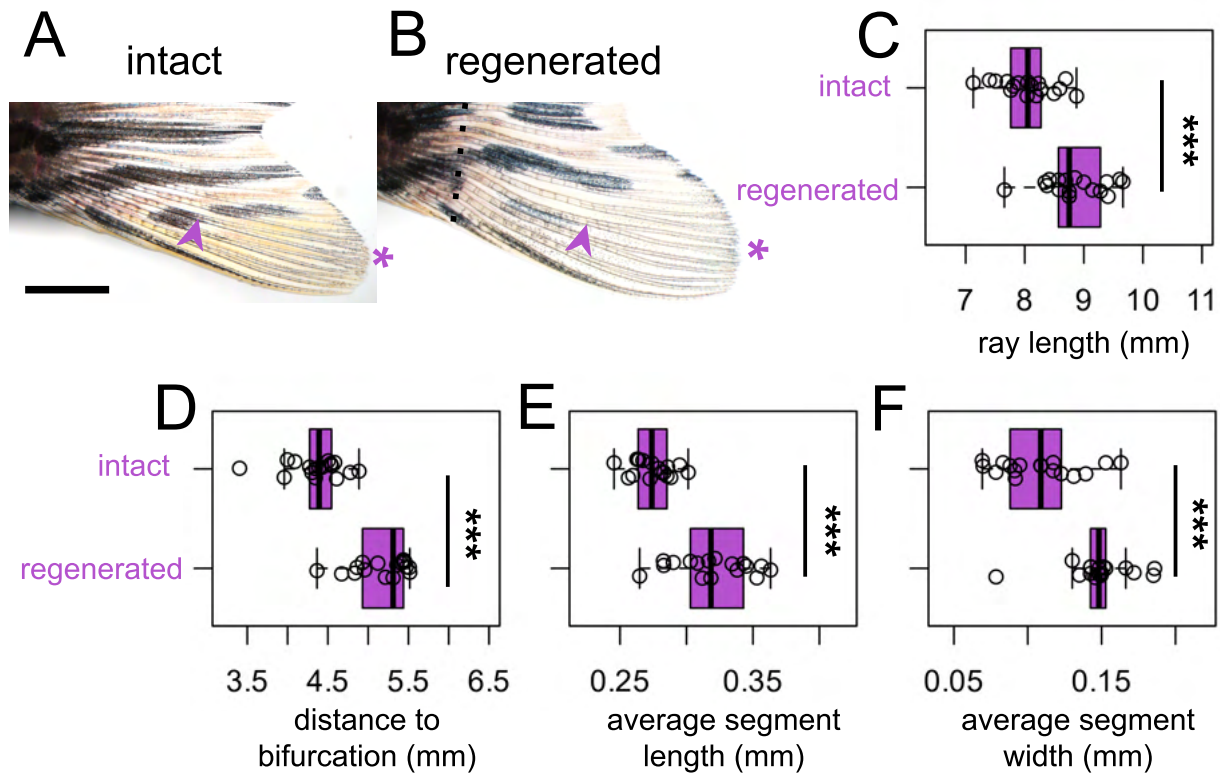
579 Significance determined by paired Welch two-sample t tests. Scale bar, 1 mm.

580



581

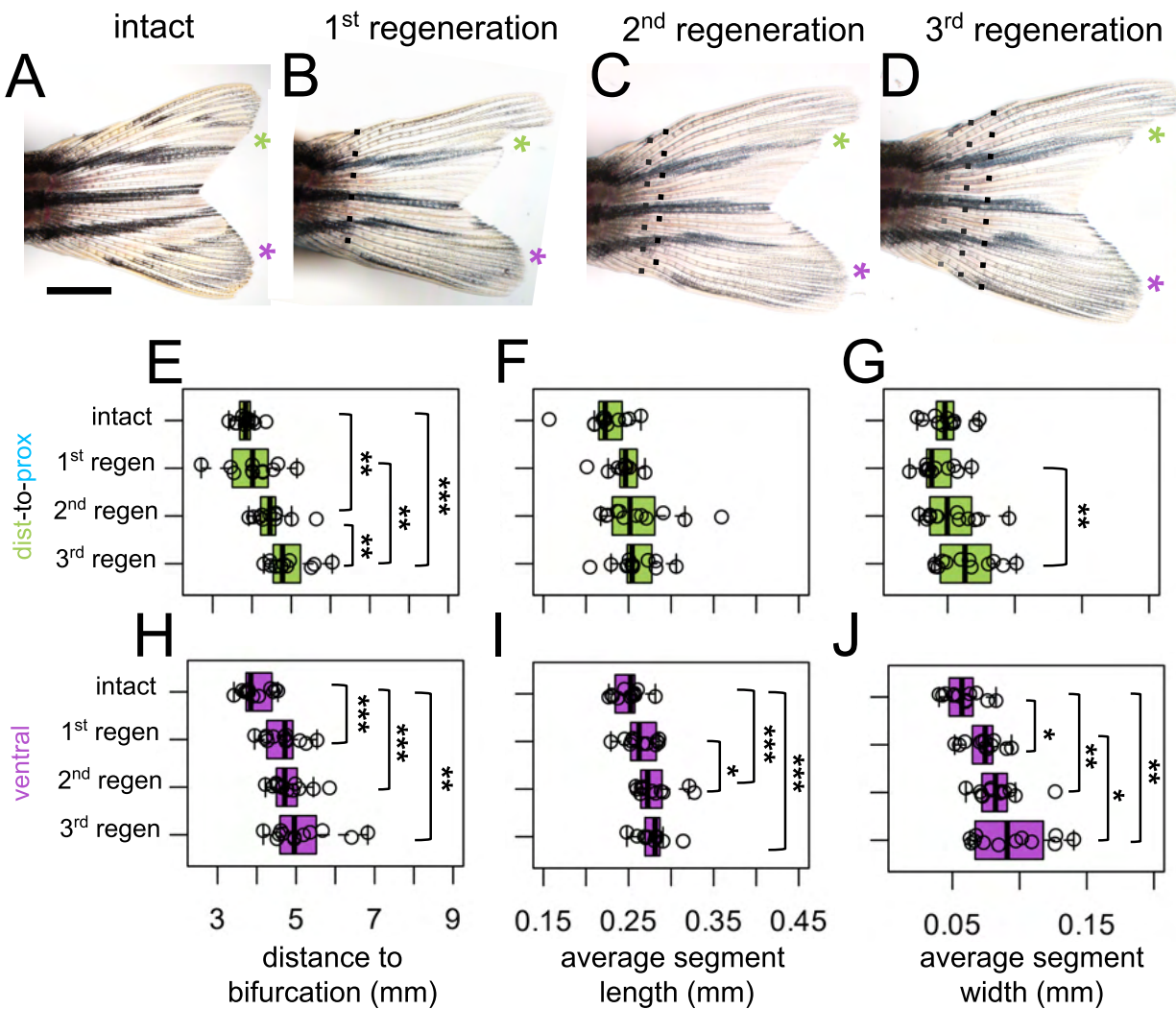
582 **Supplementary Figure 4. Dorsal ray patterning is unique from ventral ray patterning.** (A)
583 Intact fin. A yellow or purple asterisk indicates dorsal ray 4 or ventral ray 4, respectively.
584 Arrowheads, primary bifurcations. Boxplots showing the (B) total length of the ray, (C)
585 proximodistal position of the bifurcation, (D) average segment length, and (E) average segment
586 width measured from a set distance from the peduncle. Significance determined by a paired
587 Welch two-sample t test. Scale bar, 2 mm.



588

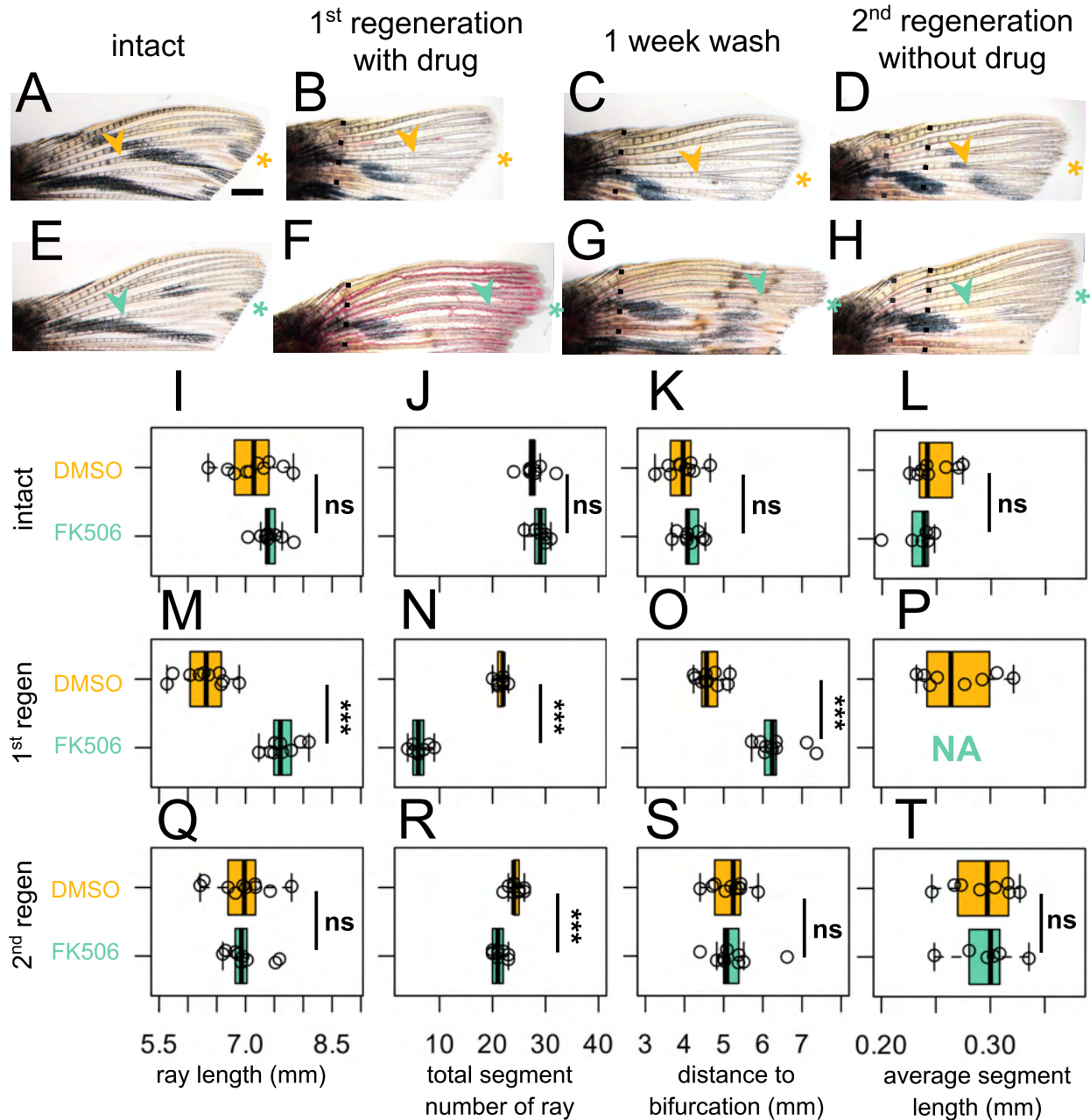
589 **Supplementary Figure 5. Intact and regenerated ray patterning are different.** (A-B) Ventral
590 lobe of (A) intact or (B) regenerating fin at 35dpa. Purple asterisks indicate ventral ray 4.
591 Arrowheads, primary bifurcations. Amputation plane, dashed line. Boxplots showing the (C) total
592 length of the ray, (D) proximodistal position of the bifurcation, (E) average segment length, and
593 (F) average segment width measured from a set distance from the peduncle. Significance
594 determined by a paired Welch two-sample t test. Scale bar, 2 mm.

595



596

597 **Supplementary Figure 6. Regenerative ray patterning differs from previous regenerated**
 598 **morphology.** (A) Intact fin. (B-D) Regenerating fin after distal-to-proximal transplantation: (B)
 599 28 days post first amputation, (C) 28 days post second amputation, (C) 28 days post third
 600 amputation. Green or purple asterisks indicate dist-to-prox or ventral ray, respectively. Black
 601 dashed line, most recent amputation. Grey dashed lines, previous amputation planes. (E, H)
 602 Boxplots showing the proximodistal position of the bifurcation. Note that bifurcations form at
 603 increasingly distal location after each amputation, as previously described. Boxplots showing
 604 (F, I) average segment length, and (G, J) average segment width. All measurements were taken
 605 from a set distance from the peduncle. Significance determined by paired repeated samples
 606 ANOVA followed by pairwise t tests. Scale bar, 2 mm.

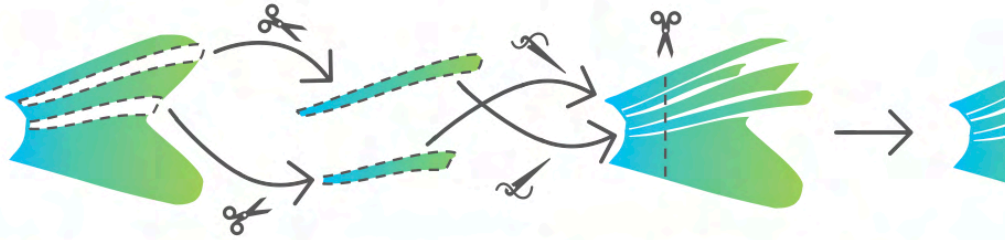


617

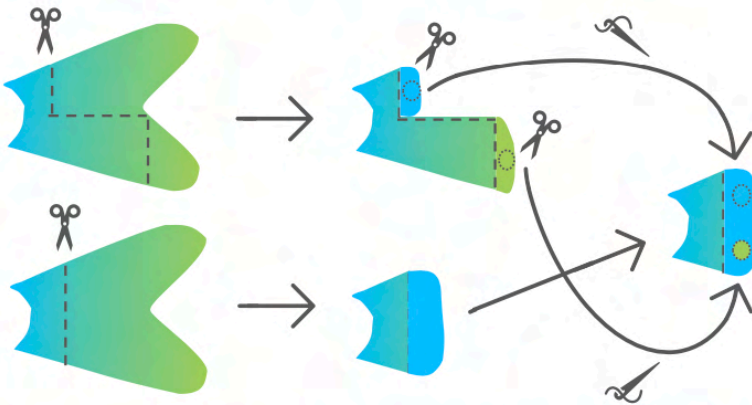
618 **Supplementary Figure 8. Calcineurin inhibition-induced morphologies are not**
619 **remembered in subsequent regeneration cycles.** (A, E) Intact dorsal lobe before treatment.
620 (B, F) Regenerated fin after (B) DMSO (yellow asterisk) or (F) 200 nM FK506 (turquoise
621 asterisk) treatment, 21 days post amputation. (C, G) Fins after one week wash to clear
622 remaining drug from water. (D, H) Regenerated fin 21 days post second amputation with no
623 treatment. Black dashed line, most recent amputation. Grey dashed lines, previous amputation
624 plane. Boxplots showing (I, M, Q) total ray length, (J, N, R) total number of segments of the ray,
625 (K, O, S) bifurcation position, and (L, P, T) average segment length for (I-L) intact, (M-P) first
626 regeneration with respective drug treatment, and (Q-T) second regeneration with no drug
627 treatment. All measurements were taken from a set distance from the peduncle. Note in (P),

628 rays were built from only ~5 segments, making segments lengths so long that none were
629 contained by the standard region of interest measured. Significance determined by unpaired
630 Welch two-sample t test. Scale bar, 1 mm.

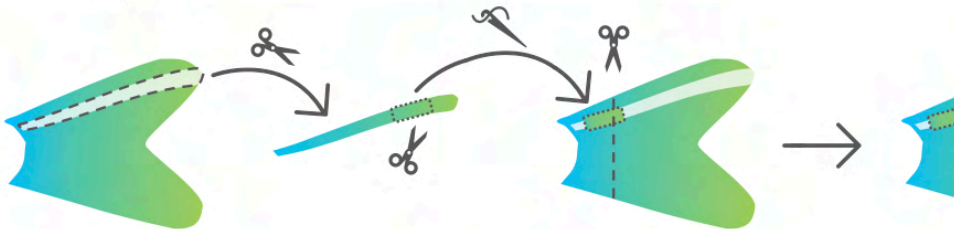
A DR3 - to - DR7's position & DR7 - to - DR3's position
(Shibata et al., 2018)



B proximal blastema - to - proximal blastema & distal blastema - to - proximal blastema
(Shibata et al., 2018)



C distal hemiray segments - to - proximal opposing hemiray
(Murciano et al., 2007)

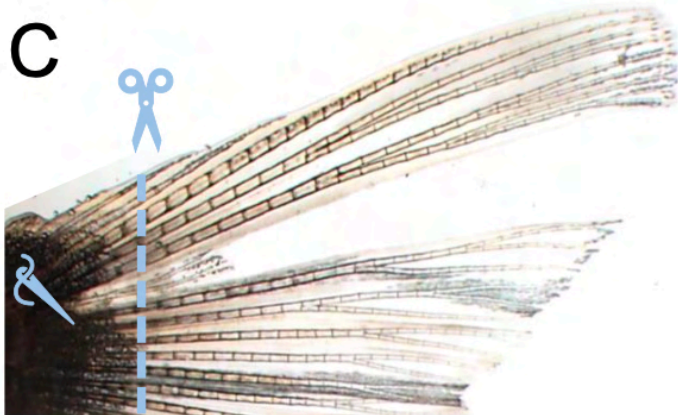
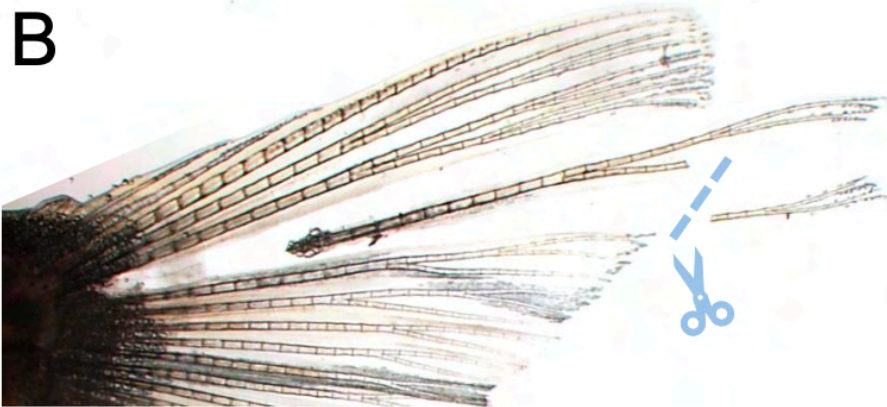
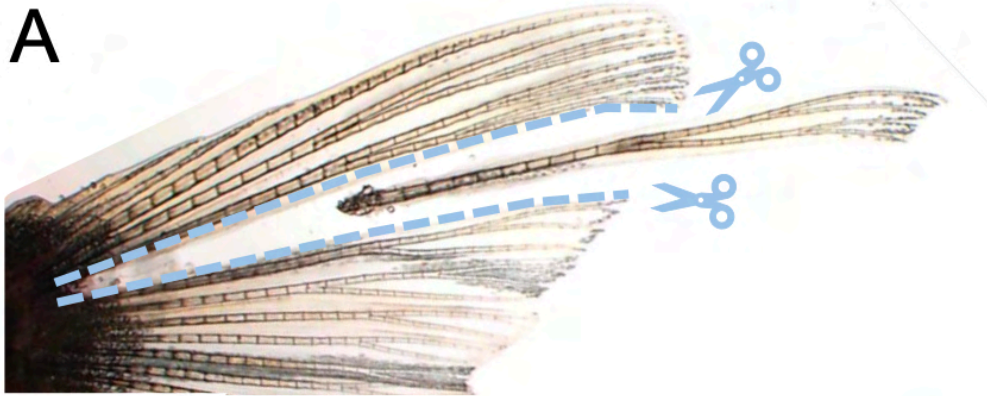


D proximal hemiray segments - to - distal opposing hemiray
(Murciano et al., 2007)



proximal  distal

632 **Supplementary Figure 9. Historical transplantation experiments.** (A) Shibata et al., 2018
633 performed full ray transplantations, moving dorsal ray 3 into dorsal ray 7 position and vice versa.
634 After successful grafting, they amputated the entire. (B) Shibata et al., 2018 also made a
635 proximal and distal amputation in a fin, collected blastema tissue from each region, and then
636 transplanted these tissues into a proximally regenerating fin. (C) Murciano et al., 2007
637 extirpated an entire distal hemiray from the fin. A distal hemiray segment was grafted onto a
638 proximal region to appose a proximal hemiray segment, then the entire fin was amputated
639 through the graft. (D) Murciano et al., 2007 further extirpated a single hemiray, then grafted a
640 proximal hemiray segment onto a distal region to appose a distal hemiray, then the entire fin
641 was amputated through the graft.



643 **Supplementary Figure 10. Distal-to-proximal transplantation.** (A) Interray tissue is cut
644 sliced on either side of dorsal ray 4, permitting the ray to be cleanly plucked out of the peduncle.
645 (B) Distal ray tissue is removed from the rest of the ray. (C-D) After allowing 24hrs for the
646 transplanted tissue to graft, the entire fin is amputated.